Intergrowth Compounds in the Zn-Rich Zn−Pd System: Toward 1D Quasicrystal Approximants

Olivier Gourdon† and Gordon J. Miller*

Department of Chemistry and Ames Laboratory, U.S. Department of Energy, Iowa State University, Ames, Iowa 50011-3111

Received November 30, 2005

A series of γ-brass related structures in the Zn-rich portion of the Zn−Pd phase diagram (ca. 80 at % Zn) is investigated using single-crystal diffraction and tight-binding electronic-structure calculations. Earlier research identified regular arrays of inversion antiphase domains (IAPDs) over a narrow composition range but did not report any characteristic superstructure(s) over the same range. Single-crystal X-ray diffraction allowed for the identification of lattice constants for six "phases" in $Zn_{1-x}Pd_x$ ($0.15 < x < 0.25$), and refinements of two crystal structures indicate two important potential building blocks for the intermediate compositions, one of these being the cubic γ-brass structure. A Farey tree construction is described that accounts for the observed long-period superlattice and provides a possible algorithm for targeting one-dimensional, quasiperiodic phases in this and related systems. Tight-binding electronic-structure calculations on the two limiting structures for this region of the Zn−Pd phase diagram suggest a relationship between structure and bonding in these complex intermetallic systems.

Introduction

The discovery of the first quasicrystal, *i*-AlMn, by Schechtman et al. in 1984[1] has energized research in the field of complex intermetallics toward uncovering other systems with structures and compositions that exhibit quasiperiodicity. Numerous quasicrystalline phases have been discovered and characterized that show icosahedral, dodecagonal, and octagonal symmetry in their diffraction patterns.[2,3] From these observations, a common practice emerged of defining quasicrystals by requiring that they possess a symmetry axis that is incompatible with translational periodicity, which eliminates any one-dimensional quasicrystals and restricts quasicrystals in two or three dimensions to possess an axis of *N*-fold symmetry, with $N = 5$ or $N > 6$.[4] Lifshitz argues that this definition is too restrictive because it excludes structures that show properties of quasicrystals without possessing forbidden symmetries. He, therefore, proposes the definition that quasicrystals are, in fact, quasiperiodic crystals, with the proviso that the crystals are strictly aperiodic, which includes one-dimensional (1D) quasicrystals.[4,5]

Although numerous quasicrystals have been identified and physically characterized, their atomic structures in real space still elude complete characterization. The noncrystallographic point symmetry of their diffraction patterns has been partially solved by the use of unconventional mathematical tools, such as higher-dimension space groups.[2,6] However, even these mathematical tools have not yet totally succeeded in determining a complete quasicrystalline structure. One way to overcome the difficulties implied by the quasiperiodicity of these phases is to synthesize and study a sequence of traditional crystalline compounds called approximants with increasing cell parameters, which converge to a quasicrystalline structure.[7,8] Examples include Bergman and Mackay phases.[9]

A number of systems showing quasicrystals and their approximants also reveal the occurrence of cubic γ-brass phases.[10−14] Further investigation strongly suggests relationships between the structure of γ-brass and quasicrystals: for example, the $[\bar{1}10]$ direction of the cubic γ-brass structure is parallel to the 10-fold axis of decagonal phases or the 5-fold axis of icosahedral phases.[13] γ-brass phases are included among Hume-Rothery phases, which are stabilized by the interaction between the Fermi surface (in the free-electron model, this is a sphere with radius k_F) and the Brillouin zone (convex polyhedra with faces located at planes perpendicular to **K**/2, where **K** is a reciprocal lattice vector).[15]

* To whom correspondence should be addressed. Tel: 515-294-6063. Fax: 515-294-0105. E-mail: gmiller@iastate.edu.

† Current Address: Lujan Neutron Scattering Center, Los Alamos National Laboratory, MSH805, Los Alamos, New Mexico 87545.

(1) Shechtman, D.; Blech, I.; Gratias, D.; Cahn, J. W. *Phys. Rev. Lett.* **1984**, *53*, 1951.
(2) Janot, C.; *Quasicrystals: A Primer*, 2nd ed.; Clarendon Press: Oxford, U.K., 1997.
(3) Stadnik, Z.; Ed., *Physical Properties of Quasicrystals*; Springer: New York, 1999.
(4) Lifshitz, R. *Found. Phys.* **2003**, *33*, 1703.
(5) Levine, D.; Steinhardt, P. J. *Phys. Rev. B* **1986**, *34*, 596.
(6) Steurer, W.; Haibach, T. In *International Tables for Crystallography, Vol. B*; Shmueli, U., Ed.; Kluwer Academic Publishers: Dordrecht, The Netherlands, 2001; pp 486−518.
(7) Lee, C.-S.; Miller, G. J. *J. Am. Chem. Soc.* **2000**, *122*, 4937.
(8) Lee, C.-S.; Miller, G. J. *Inorg. Chem.* **2001**, *40*, 338.
(9) Kim, W. J.; Gibbons, P. C.; Kelton, K. F.; Yelon, W. B. *Phys. Rev. B* **1998**, *58*, 2578.
(10) Demange, V.; Ghanbaja, J.; Machizaud, F.; Dubois, J. M. *Philos. Mag.* **2005**, *85*, 1261.
(11) Demange, V.; Milandri, A.; de Weerd, M. C.; Machizaud, F.; Jeandel, G.; Dubois, J. M. *Phys. Rev. B* **2002**, *65*, 144205.
(12) Ebalard, S.; Spaepen, F. *J. Mater. Res.* **1991**, *6*, 1641.
(13) Dong, C. *Philos. Mag. A* **1996**, *73*, 1519.
(14) Boström, M.; Hovmöller, S. J. *Solid State Chem.* **2000**, *153*, 398.

10.1021/cm0526415 CCC: $33.50
Published on Web 03/09/2006

Table 1. Summary of Approximants to the 1D Fibonacci Chain with Respect to Sequence of Fundamental Segments, Ratios of Numbers of Segments, Lengths of Unit Cells, and Valence Electrons Per Unit Cell

chain	unit cell	L:S	F_n	D_n	N_n
1	$\cdots S\cdots$	0:1	1	D_S	N_S
2	$\cdots L\cdots$	1:0	1	D_L	N_L
3	$\cdots LS\cdots$	1:1	2	$D_S + D_L$	$(N_S + N_L)/2$
4	$\cdots LSL\cdots$	2:1	3	$D_S + 2D_L$	$(N_S + 2N_L)/3$
5	$\cdots LSLLS\cdots$	3:2	5	$2D_S + 3D_L$	$(2N_S + 3N_L)/5$
6	$\cdots LSLLSLSL\cdots$	5:3	8	$3D_S + 5D_L$	$(3N_S + 5N_L)/8$
7	$\cdots LSLLSLSLLSLLS\cdots$	8:5	13	$5D_S + 8D_L$	$(5N_S + 8N_L)/13$
∞		τ:1	$F_{n-2} + F_{n-1}$		$(N_S + \tau N_L)/(\tau + 1)$

Electron-diffraction studies of γ-brass phases have shown superstructures consisting of inversion antiphase domains (IAPDs) that are sufficiently regular.[16,17] Studies of the Cu−Zn and Ni−Zn systems suggest that their dimensions vary continuously with composition so that there is no characteristic superstructure of the entire range of compositions where IAPD structures are observed.[18] Recent investigations in the Pt−Zn and Pd−Cd systems have elucidated some crystal structures that can help explain these observations.[19−22] In all cases, the direction of the superstructure is parallel with [110] for the cubic γ-brass structure, along which are found chains of icosahedra. Therefore, along this direction, 1D quasiperiodicity could exist and these IAPD structures can be explained by intergrowths of cluster units within these chains.[23]

A 1D quasiperiodic structure may be easily generated by the simple example of the Fibonacci chain.[2] The Fibonacci sequence is an automorphism: if we define two different segments, S and L, for the first generation, they become, respectively, L and LS in the next generation, which provides the algorithm to create the "quasiperiodic" chain. In the limit of the infinitely long chain, the ratio of the number of L to the number of S segments approaches the golden mean, i.e., L:$S \rightarrow \tau \approx 1.618$. Periodic chains approximating this ratio of the number of L to the number S segments involve ever-enlarging unit cells where L:$S = F_{n+1}/F_n$ and F_n is an integer in the Fibonacci sequence ($F_1 = 1$, $F_2 = 1$, and $F_{n+1} = F_n + F_{n-1}$). From a chemical perspective, the segments L and S can be distinct elements or molecular groups that will link via chemical (orbital) or physical (electrostatic or van der Waals) interactions. Such periodic chains are approximants to the quasiperiodic 1D Fibonacci chain described above. Table 1 summarizes this sequence. If the fundamental length scales of the segments L and S, respectively, are D_L and D_S, then the unit cell lengths are simply $D_n = F_{n-2}D_S + F_{n-1}D_L$. An earlier work by one of us also demonstrated that the occupied electronic states could drive the formation of such structures with optimal orbital fillings related to the corresponding electronic structures of the individual segments L and S.[24,25] Therefore, the optimal number of electrons per segment in each chain will be $N_n = (F_{n-2}N_S + F_{n-1}N_L)/F_n$, where N_S and N_L are the preferred electron counts for each segment.

In this report, we discuss the characterization of binary samples from the Zn-rich Zn−Pd system and demonstrate how the identification of two important building units can be combined via an intergrowth mechanism, diagrammed in a Farey tree, toward a possible 1D quasiperiodic structure.[23] The intergrowth structures correspond to IAPDs related to the cubic γ-brass structure already reported in the Zn−Pd and other Hume-Rothery systems.[18] These investigations in the Zn-rich portion of the Zn−Pd system and subsequent conclusions are related to the idea that a prototype 1D quasicrystal, as defined by the Fibonacci sequence, can be regarded both as a quasicrystal and as an incommensurately modulated crystal.[4] Consequently, there are two different ways to achieve the atomic structure. Perez Mato et al.[26] and Lord et al.[27] investigated this idea by trying to correlate the ordering of either vacancies or successions of octahedra/trigonal prisms with the Fibonacci sequence in their respective systems. In the Zn−Pd system, which follows Hume-Rothery's principles of electron compounds,[28] the cubic γ-brass phase is preferred for a valence electron concentration (vec = valence s, p electrons/atom ratio) of 1.61 valence s and p electrons/atom but shows a wide range in composition that varies from its published phase diagram.[29] Thus, we explored this system to investigate the relationship between structure and valence electron concentration, especially for quasiperiodic structures.

Experimental Section

Synthesis. Various $Zn_{1-x}Pd_x$ targets with compositions ranging from $x = 0.15$ to $x = 0.25$ were prepared by the same synthetic method. The elements were used as obtained: Pd (99.99%, Aldrich) and Zn (99.999%, Aldrich). All elements and products were stored and handled in an argon-filled glovebox. Reactions were carried out by heating a mixture of the elements at the appropriate molar ratio in a sealed, evacuated silica tube at 1023 K for 2 days. After naturally cooling the mixture to room temperature by turning off the furnace, we observed shiny crystals of the targeted phase. Six different, but closely related, compositions were explored in the $Zn_{1-x}Pd_x$ system.

Analysis. Single crystals that were examined by X-ray diffraction were subsequently examined by energy-dispersive X-ray spectroscopy (EDS) on a Hitachi S-2460N ESEM and gave quantitative formula in good agreement with the loaded compositions. For quantitative values, elemental Zn and Pd were used as standards. The results of the quantitative analysis agreed within 1% with the composition loaded in the silica tubes. The average value for each

(15) Asahi, R.; Sato, H.; Takeuchi, T.; Mizutani, U. *Phys. Rev. B.* **2005**, *71*, 165103.
(16) Morton, A. J. *Phys. Status Solidi A* **1974**, *23*, 275.
(17) Koyama, Y.; Hatano, M.; Tanimura, M. *Phys. Rev. B* **1996**, *53*, 11462.
(18) Morton, A. J. *Acta Metall.* **1979**, *27*, 863.
(19) Thimmaiah, S.; Richter, K. W.; Lee, S.; Harbrecht, B. *Solid State Sci.* **2003**, *5*, 1309.
(20) Harbrecht, B.; Thimmaiah, S.; Armbrüster, M.; Pietzonka, C.; Lee, S. *Z. Anorg. Allg. Chem.* **2002**, *628*, 2744.
(21) Thimmaiah, S.; Conrad, M.; Lee, S.; Harbrecht, B. *Z. Anorg. Allg. Chem.* **2004**, *630*, 1762.
(22) Schmidt, J. T.; Lee, S.; Fredrickson, D. C.; Conrad, M.; Sun, J.; Harbrecht, B.; Stephens, P. W.; private communication, 2005.
(23) Gourdon, O.; Izaola, Z.; Elcoro, L.; Petricek, V.; Miller, G. J. *Philos. Mag.* **2006**, *86* (3−5) 419−425.
(24) Burdett, J. K.; Miller, G. J. *Inorg. Chem.* **1986**, *25*, 4069.
(25) Maciá, E.; Domínguez-Adame, F. *Physica B* **1995**, *216*, 53.
(26) Perez-Mato, J. M.; Zakhour-Nakhl, M.; Weill, F.; Darriet, J. *J. Mater. Chem.* **1999**, *9*, 2795−2808.
(27) Lord, E. A.; Ranganathan, S.; Subramaniam, S. A. *Philos. Mag. A* **2002**, *82* (2), 255−268.
(28) Hume-Rothery, W. *J. Inst. Metals* **1926**, *35*, 309.
(29) Massalski, T. B., Ed. *Binary Alloy Phase Diagrams*, 2nd ed.; ASM International: Materials Park, OH, 1990; Vol. 3, p 3068.

Table 2. Compositions, Valence s and p Electron Concentrations, Structural Parameters, and Periodicities of the Subnetworks for Different $Zn_{1-x}Pd_x$ ($x = 0.15-0.25$) Intergrowth Compounds[a]

composition (loaded)	$Zn_{82}Pd_{18}$	$Zn_{79}Pd_{21}$	$Zn_{78}Pd_{22}$	$Zn_{77.5}Pd_{22.5}$	$Zn_{77}Pd_{23}$	$Zn_{75}Pd_{25}$
EDS results	$Zn_{82.1(6)}Pd_{17.9}$	$Zn_{79.6(6)}Pd_{20.4}$	$Zn_{78.2(6)}Pd_{21.8}$	$Zn_{77.7(6)}Pd_{22.3}$	$Zn_{77.2(5)}Pd_{22.8}$	$Zn_{75.4(6)}Pd_{24.6}$
valence s and p electrons	1.642	1.592	1.564	1.554	1.544	1.508
composition (refined)	$Zn_{81.9}Pd_{18.1}$					$Zn_{75.8}Pd_{24.2}$
no. of measured reflns	3239	107 721	48 515	68 759	152 623	15 929
a_{orth} (Å)	12.912(6)	12.919(8)	12.909(5)	12.927(7)	12.915(4)	12.929(3)
b_{orth} (Å)	9.0906(3)	9.091(6)	9.115(3)	9.120(9)	9.114(3)	9.112(4)
c_{orth} (Å)	12.912(6)	106.86(6)	46.894(5)	80.98(5)	146.10(13)	33.32(1)
space group	*Fm*2*m*					*Cmce*
V (Å^3)	1515.6(9)	12550.3(9)	5517.8(9)	9547.1(9)	17197.0(9)	3925.4(9)
m/*n*	5/3	*41/25*	*18/11*	*31/19*	*57/35*	13/8
estimated *c* param[b] (Å)	12.9	*107.5*	*47.3*	*81.7*	*150.5*	34.4
estimated *c* param[c] (Å)	12.912	*105.376*	*46.232*	*79.552*	*146.192*	33.32
V/atom (Å^3)	14.45	*14.32*	*14.28*	*14.25*	*14.23*	14.22
no. of atoms/cell	52	*876*	*386*	*670*	*1208*	276
clusters (n_S: $2n_L$)	1:0	*3:4*	*1:2*	*1:4*	*1:8*	0:2
N_x	1.642	*1.588*	*1.575*	*1.553*	*1.534*	1.508

[a] Information presented in italics indicates estimates based upon theoretical and structural models described in the text. See text for discussion of various parts of this table. [b] $c = 4.3n$ Å. [c] $c = (12.912n_S + 33.32n_L)$ Å.

sample, which is listed in Table 2, was obtained from 10 points measured in different locations for each sample.

Diffraction. Room temperature (ca. 300 K) data collections were carried out for all phases on single crystals using a Bruker SMART 1000 CCD diffractometer with Mo Kα radiation ($\lambda = 0.71073$ Å) and a detector-to-crystal distance of 5.08 cm. Crystals were selected and mounted at the ends of glass fibers within epoxy. Data were collected in a full hemisphere and harvested by collecting three sets of frames within 0.3° scans in ω for an exposure time of 10 s per frame. The range of 2θ extended from 4.0 to 57.0°. Unit cell parameters were determined by indexing 200−999 reflections and then refined using all observed Bragg reflections after integration. Thereafter, the reflection intensities were integrated with the *SAINT* subprogram in the *SMART* software package.[30] The intensities were adjusted for Lorentz polarization and corrected for absorption via a Gaussian analytical method, and the crystal shapes and dimensions were optimized with the STOE *X-Shape* program[31] on the basis of equivalent reflections. All data treatments, refinements, and Fourier syntheses were carried out using the *SIR97* and *JANA2000* program packages.[32,33]

Electronic Structure. Tight-binding linear muffin-tin orbital (TB-LMTO) electronic-structure calculations were carried out for $Zn_{11}Pd_2$ and $Zn_{53}Pd_{16}$ in the atomic sphere approximation (ASA)[34] using the *LMTO* program, version 4.7.[35] Exchange and correlation were treated in a local density approximation.[36] All relativistic effects except spin−orbit coupling were taken into account using a scalar relativistic approximation.[37] The radii of the Wigner−Seitz (WS) spheres were obtained by requiring that the overlapping potential be the best possible approximation of the full potential according to an automatic procedure; no empty spheres were necessary.[38] The WS radii determined by this procedure for Pd and Zn in these two compounds ranged, respectively, between 1.48 and 1.52 Å and 1.48 and1.57 Å. The basis set for these calculations included Pd 5s, 5p, and 4d and Zn 4s, 4p, and 3d orbitals. The k-space integrations to determine the self-consistent charge density, density of states, and crystal Hamiltonian orbital populations (COHP) were performed by the tetrahedron method[39] using 172 and 52 k-points, respectively, in the irreducible wedges of the unit cells of $Zn_{11}Pd_2$ (cubic) and $Zn_{53}Pd_{16}$ (orthorhombic).

Results

Among the six samples that were investigated by single-crystal X-ray diffraction experiments, those that exceeded 20 at % Pd (five out of six samples) gave data sets that were consistent with orthorhombic symmetry and could be indexed with either an *F*- or *C*-centered orthorhombic Bravais lattice. The one sample below 20 at % Pd was solved as a cubic γ-brass phase, space group $I\bar{4}3m$ and lattice constant ca. 9.1 Å. Transformation of this cubic unit cell according to $a \rightarrow a_{orth} = a - c$, $b \rightarrow b_{orth} = b$, and $c \rightarrow c_{orth} = a + c$ provides a consistent orthorhombic description of this phase with cell parameters $a \approx 12.9$ Å, $b \approx 9.1$ Å, and $c \approx 12.9$ Å and space group *Fm*2*m*, a subgroup of $I\bar{4}3m$. All six phases now show similar length scales along the orthorhombic a_{orth} and b_{orth} directions as, respectively, 12.9 and 9.1 Å, whereas the orthorhombic c_{orth} direction can be described as 4.3*n* Å, where *n* is an integer defining the Pd network periodicity. $Zn_{10.65}Pd_{2.35}$ ($x = 0.181$ in $Zn_{1-x}Pd_x$) represents the case $n = 3$, where the *a* and *c* parameters are equal and additional symmetry operations exist that lead to cubic symmetry. The misfit character of all the structures with two distinct main subsets and satellite reflections is clear from their corresponding diffraction patterns (see Figure 1). For example, primary *hkl* reflections are observed for $l = 8$ and $l = 13$ in the case of $Zn_{52.32}Pd_{16.68}$ ($x = 0.242$). Table 2 summarizes the lattice constants and some structural and electronic characterizations of these six samples.

Among these six products, the two compounds at the highest and lowest Pd concentrations could be refined by standard single-crystal X-ray diffraction methods. The main

(30) *SMART*; Bruker AXS, Inc.: Madison, WI, 1996.
(31) *X-Shape: Crystal Optimization for Numerical Absorption Correction*; STOE & CIE GmbH: Darmstadt, Germany, 1996.
(32) Altomare, A.; Burla M. C.; Camalli, M.; Cascarano, G.; Giacovazzo, C.; Guagliardi, A.; Moliterni, A. G. G.; Polidori, G.; Spagna, R. *SIR97: A New Program for Solving and Refining Crystal Structures*; *J. Appl. Cryst.* **1998**, *32*, 115−119.
(33) Petricek, V.; Dusek, M. *The Crystallographic Computing System JANA2000*. Institute of Physics: Praha, Czech Republic, 2000.
(34) Andersen, O. K. *Phys. Rev. B* **1986**, *34*, 2439.
(35) Krier, G.; Jepsen, O.; Burkhardt, A.; Andersen, O. K. *Tight-Binding LMTO*, version 4.7; Max-Planck-Institut für Festkörperforschung: Stuttgart, Germany, 1997.
(36) von Barth, U. Hedin, L. *J. Phys. C* **1972**, *5*, 1629.
(37) Koelling, D. Harmon, B. N. *J. Phys. C* **1977**, *10*, 3107.
(38) Jepsen, O.; Andersen, O. K. *Z. Phys. B* **1995**, *97*, 645.
(39) Blöchl, P. E.; Jepsen, O.; Andersen, O. K. *Phys. Rev. B* **1994**, *49*, 16223.

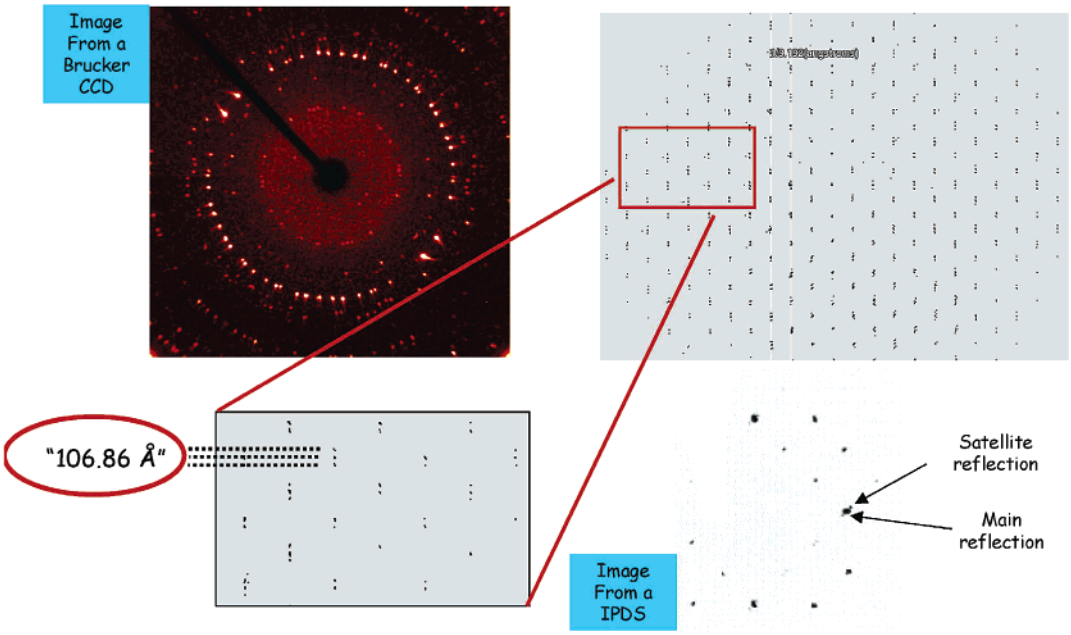

Figure 1. Diffraction patterns observed for $Zn_{79}Pd_{21}$ using two different diffractometers (Bruker Apex and Stoe IPDS). The main reflections may be indexed according to the cubic γ-brass unit cell, whereas the satellite reflections are in agreement with a long-period superlattice formation with orthorhombic symmetry. In this particular case, the long period may be estimated to be 106.86(6) Å.

Table 3. Crystallographic Data for $Zn_{10.65}Pd_{2.35}$ ($Zn_{81.9}Pd_{18.1}$).

formula	$Zn_{10.65}Pd_{2.35}$
mol wt (g mol^{-1})	946.42
cryst syst	cubic
space group	$I\bar{4}3m$
T (K)	293(2) K
a (Å)	9.0906(3)
V (Å^3)	751.238(3)
Z	4
d_{calcd} (Mg m^{-3})	8.9807
cryst description	needle
cryst size (mm^3)	0.5 × 0.2 × 0.1
diffractometer	Bruker SMART Apex
radiation	Mo
no. of measured reflns	3239
index ranges	$-6 < h < 6$, $-8 < k < 8$, $-12 < l < 12$
θ range for data collection (deg)	2.39−24.05
linear abs coeff (mm^{-1})	41.530
abs corr	analytical
criterion for observed reflns	2σ
R_{int} (obs)	0.0379
refinement method	Full-matrix least-squares on F^2
F(000)	1710
no. of independent reflns	2955 [R(int) = 0.0379]
data/restraints/params	200/0/19
GOF on F^2	1.33
final R indices [$I > 2\sigma(I)$]	R1 = 0.0129, wR2 = 0.0268
extinction coeff	0.026(2)
largest diff. peak and hole (e$^-$/Å^3)	0.53 and −0.76

Table 4. Fractional Atomic Coordinates, Site Occupation Factors, and Isotropic Equivalent Displacement Parameters U_{Eq} (Å^2) for $Zn_{10.65}Pd_{2.35}$.

	Wyckoff site	SOF Zn/Pd	x	y	z	U_{eq}
Pd1	8*c*		0.82677(3)	0.82677(3)	0.82677(3)	0.0079(1)
Zn2	8*c*		0.10866(6)	0.89134(6)	0.89134(6)	0.0130(1)
M3	12*e*	0.882(6)/0.118	0.64243(7)	0	0	0.0105(2)
Zn4	24*g*		0.53889(6)	−0.18905(4)	−0.18905(4)	0.0132(1)

crystallographic data, atomic coordinates, crystallographic site occupancies, and temperature displacement parameters are summarized in Tables 3−6.

$Zn_{10.65}Pd_{2.35}$ ($Zn_{0.819}Pd_{0.181}$) crystallizes in the well-known cubic γ-brass phase that exists for a variety of Hume-Rothery

Table 5. Crystallographic Data for $Zn_{52.32}Pd_{16.68}$ ($Zn_{75.8}Pd_{24.2}$).

formula	$Zn_{52.32}Pd_{16.68}$
mol wt (g mol^{-1})	5195.47
cryst syst	orthorhombic
space group	*Cmce*
T (K)	293(2)
a (Å)	12.929 (3)
b (Å)	9.112 (4)
c (Å)	33.32 (1)
V (Å^3)	3925.4(9)
Z	4
d_{calcd} (Mg/m^3)	8.7884
cryst description	needle
cryst size (mm^3)	0.4 × 0.1 × 0.1
Diffractometer	Bruker Smart Apex
radiation	Mo
no. of measured reflns	15 929
index ranges	$-13 < h$ 177408n, $-10 < k < 10$, $-38 < l < 38$
θ range for collection (deg)	2.39−24.05
Linear abs coeff (mm^{-1})	38.653
abs corr	analytical
criterion for obs reflns	2σ
R_{int} (obs)	0.0402
refinement method	full-matrix least -squares on F^2
F(000)	9240
no. of independent reflns	1184
data/restraints/params	1184/0/178
GOF on F^2	1.46
Final R indices [$I > 2\sigma(I)$]	R1 = 0.0288, wR2 = 0.0385
extinction coeff	0.000163(9)
largest diff. peak and hole (e$^-$/Å^3)	1.97 and −2.75

intermetallic systems, such as Ni−Zn (Ni_2Zn_{11})[40] or Fe−Zn (Fe_3Zn_{10}).[41] Our results nearly agree with an earlier crystal structure solution from Edstrom et al., which concluded a composition between $Zn_{0.81}Pd_{0.19}$ ($Zn_{10.5}Pd_{2.5}$) and $Zn_{0.77}Pd_{0.23}$ ($Zn_{10}Pd_3$).[42] The cubic γ-brass structure for $Zn_{10.65}Pd_{2.35}$ is

(40) Johansson, A.; Ljung, H.; Westman, S. *Acta Chem. Scand.* **1968**, *22*, 2743.
(41) Belin, C. H. E.; Belin, R. C. H. *J. Solid State Chem.* **2000**, *151*, 85.
(42) Edström, V.-A.; Westman, S. *Acta Chem. Scand.* **1969**, *23*, 279.

Table 6. Fractional Atomic Coordinates, Site Occupation Factors, and Equivalent Displacement Parameters U_{Eq} (Å^2) for $Zn_{52.32}Pd_{16.68}$

	Wyckoff site	SOF Zn/Pd	*x*	*y*	*z*	U_{eq}
Zn1	4*a*		0	0	0	0.0153(1)
Zn2	8*f*		0	0.04024(3)	0.07885(3)	0.0123(2)
Zn3	8*f*		0	−0.05148(3)	0.15548(5)	0.0080(1)
Zn4	8*f*		0	0.05184(4)	0.22720(5)	0.0113(1)
Zn5	8*f*		0	−0.01080(5)	0.30666(6)	0.0114(2)
Zn6	8*f*		0	−0.02527(3)	0.38619(6)	0.0118(1)
Zn7	8*f*		0	0.05368(5)	0.46359(7)	0.0087(2)
Pd8	8*f*		0	0.27203(5)	0.03098(6)	0.0081(1)
Pd9	8*f*		0	0.23873(6)	0.15657(5)	0.0115(2)
Pd10	8*f*		0	0.26657(4)	0.28086(5)	0.0110(2)
Pd11	8*f*		0	0.25696(4)	0.40658(4)	0.0090(2)
Zn12	16*g*		0.12872(3)	0.26222(4)	0.09303(3)	0.0122(2)
Zn13	16*g*		0.12731(4)	0.28331(5)	0.22024(5)	0.0102(1)
Zn14	16*g*		0.11658(5)	0.20586(5)	0.34407(3)	0.0098(1)
Zn15	16*g*		0.12120(5)	0.29429(6)	0.46767(5)	0.0117(2)
M16	16*g*	0.89(1)/0.11	0.17639(6)	0.59381(5)	0.08746(5)	0.0124(1)
M17	16*g*	0.69(1)/0.31	0.17763(7)	0.59341(5)	0.22429(6)	0.0090(1)
Zn18	16*g*		0.18608(5)	0.62713(3)	0.34129(5)	0.0131(2)
M19	16*g*	0.17(1)/0.83	0.17843(5)	0.58617(8)	0.46449(5)	0.0073(1)
Zn20	16*g*		0.17672(5)	0.59473(8)	0.60148(4)	0.0078(2)
Zn21	16*g*		0.17996(4)	0.60215(7)	0.71031(4)	0.0155(2)
M22	16*g*	0.08(1)/0.92	0.17851(5)	0.57886(6)	0.84530(3)	0.0077(1)
Zn23	16*g*		0.18381(6)	0.61574(6)	0.97540(6)	0.0112(1)

Table 7. Interatomic Distances in $Zn_{10.65}Pd_{2.35}$ and $Zn_{52.32}Pd_{16.68}$ as Determined from Single-Crystal X-ray Diffraction Experiments

$Zn_{10.65}Pd_{2.35}$			$Zn_{52.32}Pd_{16.68}$		
Pd1 (CN12)	Zn2	2.6937(6) (×3)	Pd (CN12)	Zn	2.5728(7) to 2.7916(8)
	M3	2.7871(5) (×3)		M19	2.8658(7)
	Zn4	2.6249(6) (×6			
M3 (CN11)	Zn2	2.6592(7) (×2)	Pd9 (CN11)	Zn	2.5796(15) to 2.7157(19)
	M3	2.5896(8)		M22	2.8449 (7)
	Zn4	2.6063(5) (×2)			
		2.8801(4) (×4)			
		2.7868(6) (×2)			
other Zn−Zn distances		2.6768(7)−2.7940(8)	other Zn−Zn distances		2.5681(7)−2.8342(8)

illustrated from various perspectives in Figure 2. The most traditional description involves the 26-atom cluster constructed from successive polyhedral shells: (a) an inner tetrahedron of Zn atoms; (b) an outer tetrahedron of Pd atoms; (c) an octahedron of Zn/Pd atoms, and (d) a distorted cuboctahedron of Zn atoms. These clusters form a body-centered cubic packing; this classical description begins from a 3 × 3 × 3 superstructure of a bcc packing of atoms followed by removing 2 atoms from the 54-atom supercell (one from the corner, one from the center of the supercell) and then shifting the remaining atomic sites to the resulting coordinates. Explanation of the existence and stability of this cubic γ-brass structure has received much attention, and the Jones−Hume-Rothery mechanism of interaction between the Fermi sphere and the Brillouin zone planes (330) and (411) has been theoretically verified through recent electronic-structure calculations.[15] On the other hand, the viewpoint as a distorted "defect-bcc" structure has been contested by first principles total energy calculations of various structural models.[43] Therefore, we can also view the cubic γ-brass structure of $Zn_{10.65}Pd_{2.35}$ as being constructed from a cluster of four interpenetrating Pd-centered icosahedra,[44] which can

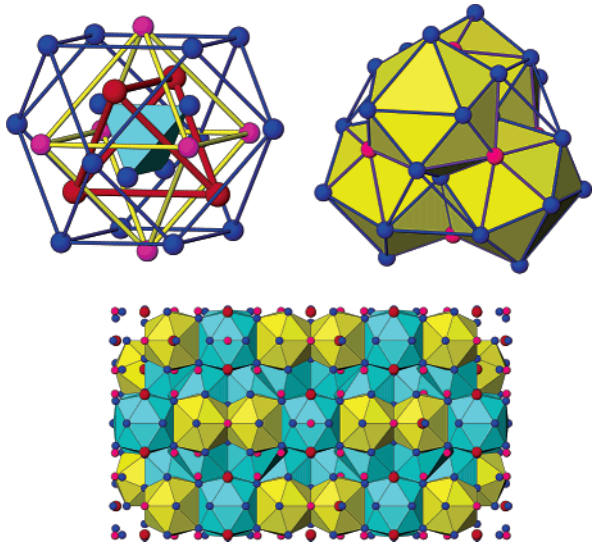

Figure 2. Representations of the cubic γ-brass structure of $Zn_{10.65}Pd_{2.35}$. Blue spheres, Zn atoms; red spheres, Pd atoms; purple spheres, mixed Pd/Zn sites. Top left: 26-atom cluster that forms a bcc-type packing, with an emphasis on the different polyhedra. Top right: Four condensed Pd-centered icosahedra. Bottom: (010) projection of the γ-brass structure. Horizontal direction is [101] and emphasizes the Pd- and M-centered polyhedra.

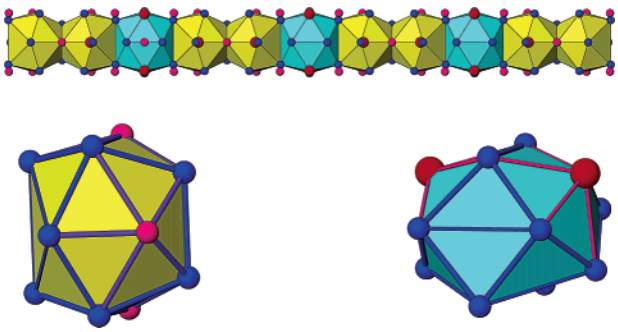

Figure 3. Top: chain along [110] in the γ-brass structure of $Zn_{10.65}Pd_{2.35}$. Yellow icosahedra are Pd-centered; blue icosahedra are (Pd/Zn)-centered and involve two Pd sites. Bottom left: $[Zn_8M_4]$Pd-centered icosahedron. Bottom right: $[Zn_{10}Pd_2]$M-centered distorted icosahedron.

be formulated as $[Pd^{(8c)}(Zn_{3/3}^{(8c)}\ M_{3/2}^{(12e)}\ Zn_{6/2}^{(24g)})]_4$. Zn atoms exclusively occupy the convex vertexes of this cluster, whereas the concave vertexes refine as a mixture of Pd (ca. 11%) and Zn (ca. 89%) atoms. Pd−Zn/M distances range between 2.590 and 2.880 Å, whereas the shortest distance in this structure, 2.590 Å, occurs between pairs of M sites. Significant distances are summarized in Table 7.

Figure 2 also shows the importance of these clusters for the extended γ-brass structure; pairs of face-sharing Pd-centered icosahedra form chains along {110} directions of the cubic cell. These clusters are connected by polyhedra centered by the M sites. These chains are emphasized in Figure 3, and we will return to this perspective in a subsequent section.

On the other hand, the structure of $Zn_{52.32}Pd_{16.68}$ is closely related to the $NiZn_3$ structure refined by Nover et al. in 1980[45] and recently reexamined by Lee and Harbrecht et al.[46] as part of investigations on Vernier structures and other complex intermetallics. The structure is illustrated in Figure 4 and

(43) Paxton, A. T.; Methfessel, M.; Pettifor, D. G. *Proc. R. Soc. London, Ser. A* **1997**, *453*, 1493.

(44) Lord, E. A.; Ranganathan, S. *J. Non-Cryst. Solids* **2004**, *334−335*, 121.

(45) Nover, G.; Schubert, K. *J. Less-Common Met.* **1980**, *75*, 51.

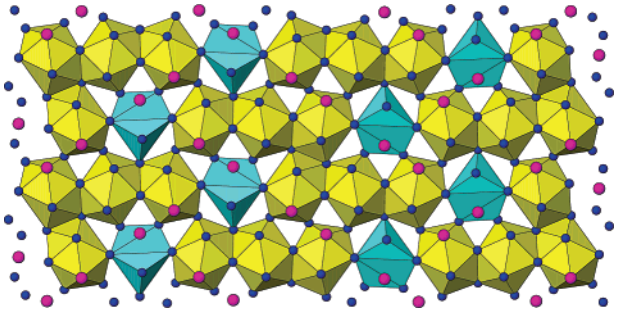

Figure 4. (100) projection of $Zn_{52.32}Pd_{16.68}$.

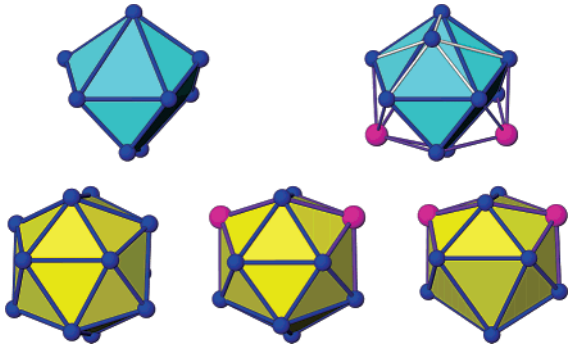

Figure 5. Polyhedra surrounding the Pd atoms in the structure of $Zn_{52.32}Pd_{16.68}$ as determined by single-crystal X-ray diffraction. Top: $[Zn_9]Pd$ cage, which is an icosahedron missing two vertexes (surrounding Pd9 sites); $[Zn_9M_2]Pd$ cage showing the distorted icosahedron. Bottom: Various icosahedra making up the three face-sharing icosahedra. From left to right, these polyhedra coordinate, respectively, Pd8, Pd10, and Pd11 sites. The $[Zn_{12}]Pd$ cluster centers all TI segments.

highlights the chains of Pd-centered polyhedra along the crystallographic *c* direction. $Zn_{52.32}Pd_{16.68}$ shows clusters of three consecutive face-sharing Pd-centered icosahedra. The middle icosahedron involves just Zn atoms, whereas the two terminal icosahedra show two sites with mixed Zn/Pd occupancies. The centering atoms are exclusively Pd sites. Under complete segregation of the elements, the expected composition would be $Zn_{49}Pd_{20}$, which is more Pd-rich than these phases allow (close to 28 at % Pd), as confirmed by electronic-structure calculations (see below). These clusters are connected by Pd-centered 11-vertex polyhedra when a distance limit is set at 2.90 Å. If a slightly larger distance criterion is used (e.g., less than 3.00 Å), then this polyhedron is a distorted icosahedron. These polyhedra are illustrated in Figure 5. Important distances for these clusters are summarized in Table 7. The primitive unit cell contains two equivalent chains.

Analysis of the crystal structures of $Zn_{0.819}Pd_{0.181}$ and $Zn_{0.758}Pd_{0.242}$ shows that the volume per atom increases with the concentration of Zn. Although this result may seem counterintuitive, in fact, the ground-state atomic volumes for hcp Zn and fcc Pd, respectively, are 15.21 and 14.72 Å^3. Furthermore, all atomic volumes in this study lie well below these elemental values and are consistent with reported unit cell volumes for other compounds in the Zn−Pd binary system:[47] (i) $ZnPd_2$ (oP12, 14.12 Å^3/atom); (ii) ZnPd (tP4, 14.06 Å^3/atom); (iii) Zn_3Pd_2 (cP2, 14.10 Å^3/atom); and (iv)

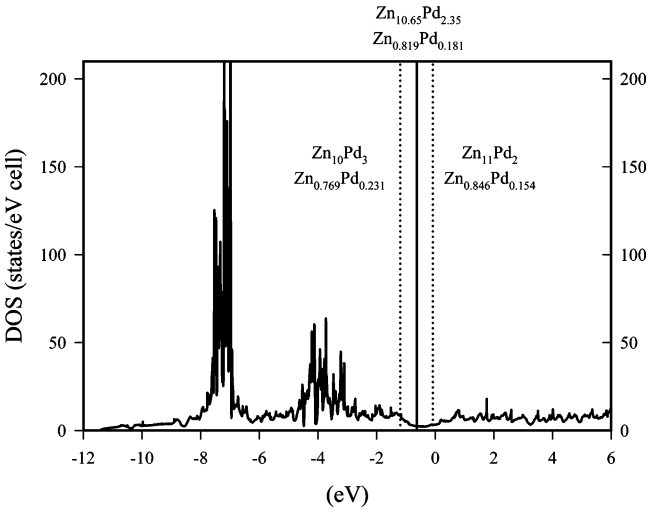

Figure 6. Total density of states for $Zn_{11}Pd_2$ from TB-LMTO-ASA calculations. The Fermi level for the observed composition ($Zn_{10.65}Pd_{2.35}$), assuming a rigid-band approximation, is shown by the solid vertical line; the corresponding Fermi levels for $Zn_{11}Pd_2$ and $Zn_{10}Pd_3$ are shown by dotted lines. The large peak just above −8 eV is mostly Zn 3d orbitals; the broader peak near −4 eV is mostly Pd 4d orbitals. A pseudogap is evident near the calculated Fermi levels.

Zn_2Pd (oC48, 14.21 Å^3/atom). The relationship between atomic volumes in the ground-state structures for Zn and Pd can be understood from their respective electronic structures. For hcp Zn, the filled energy bands lead to an approximate electronic configuration of $3d^{10}4s^{2-n}4p^n$; all Zn−Zn bonding arises from occupation of the valence 4s and 4p bands, whereas the formally filled 3d band reduces these orbital interactions through filled-orbital repulsions.[48] On the other hand, fcc Pd shows $4d^{10-n}5s^n$ with the 5p band essentially empty. Transfer of valence electrons from the 4d band into the 5s band depletes some Pd−Pd d−d antibonding orbitals and contributes to shorter, stronger interactions:[49] ΔH_f^0 (Pd, g) = 377 kJ/mol; ΔH_f^0 (Zn, g) = 129.3 kJ/mol.[50] The smaller volumes for the Zn−Pd intermetallic compounds imply stronger heteroatomic Pd−Zn bonding than homoatomic Pd−Pd or Zn−Zn bonding, and we will discuss this in the next section. Such compression in volumes is evident among Zintl phases and other polar intermetallic compounds, which involve metallic or semimetallic elements with significantly different electronegativities.[51]

Electronic Structure. Figure 6 shows the electronic density of states calculated for $Zn_{11}Pd_2$. Note the pseudogap at the Fermi level for $Zn_{10.65}Pd_{2.35}$, which is in excellent agreement with results from other calculations on, for example, Cu_5Zn_8 and Cu_9Al_4.[15] The range of the pseudogap occurs for vec = 1.538−1.692 valence s and p electrons per atom. In this DOS, the Pd 4d band is ca. 3 eV below the Fermi level; Zn 3d bands occur 8−10 eV below Fermi. To

(46) S. Lee. *Abstracts of Papers*, 36th Middle Atlantic Regional Meeting of the American Chemical Society, Princeton, NJ, June 8−11, 2003;American Chemical Society: Washington, DC.

(47) Villars, P.; Calvert, L. D. *Pearson's Handbook of Crystallographic Data for Intermetallic Phases*, 2nd ed.; ASM International: Materials Park, OH, 1991.

(48) Häussermann, U.; Simak, S. I. *Phys. Rev. B* **2001**, *64*, 245114.

(49) Gourdon, O.; Gout, D.; Miller, G. J. *Encyclopedia of Condensed Matter Physics*; Elsevier: Amsterdam, 2005; p 409.

(50) Greenwood, N. N.; Earnshaw, A. *Chemistry of the Elements*; Pergamon Press: Oxford, UK, 1984.

(51) Miller, G. J.; Lee, C.-S.; Choe, W. In *Highlights in Inorganic Chemistry*; Meyer, G., Ed.; Wiley-VCH: Heidelberg, Germany, 2002; p 21.

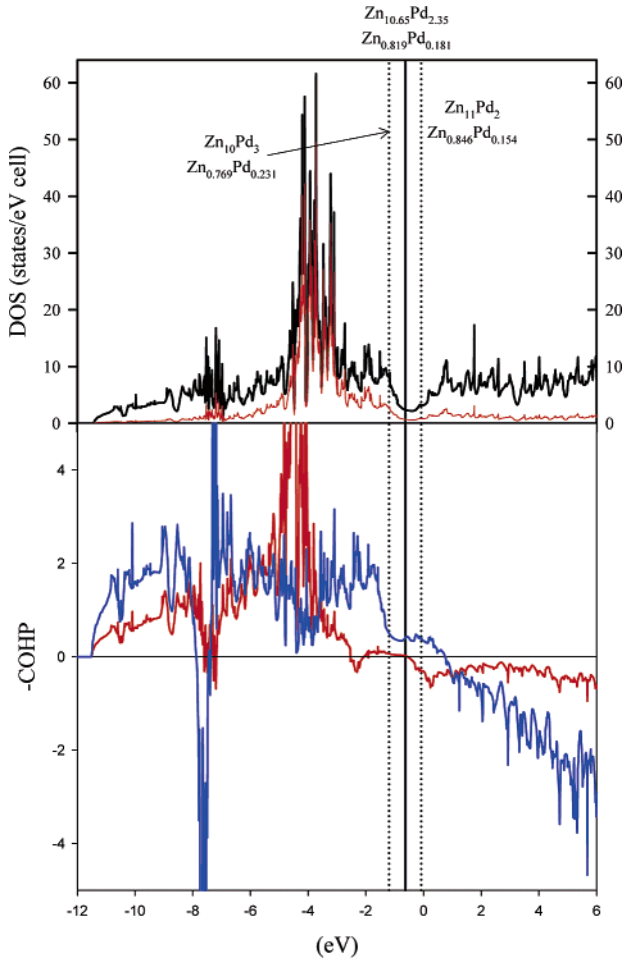

Figure 7. Total DOS (top) and −COHP (bottom) curves for $Zn_{11}Pd_2$. The Zn 3d orbitals are not included in either curve so that the states close to the Fermi levels can be emphasized. Pd orbitals are shown by the red curve. For the −COHP curves, blue = Zn−Zn interactions and red = Zn−Pd interactions.

examine the site preference for Pd among the four crystallographic sites, we carried out calculations using mixed sites, and there Pd has a strong preference for fully occupying the observed 16b sites with the next being the 24e sites. In a recent work, Schmidt et al. used relative Mulliken populations as calculated from semiempirical calculations to show that these two sites are preferred for the more electronegative element in the intermetallic.[22] Is Pd more electronegative than Zn? As measured from configuration energies,[52] this is indeed the case, although these values are extremely close: CE(Pd) = 9.402 eV, CE(Zn) = 9.395 eV (Pauling electronegativities are more widely separated: 2.2 eV for Pd, 1.65 eV for Zn[50]). These values can be attributed to the variation in valence d orbital energies across the 3d and 4d series. It is also of interest that the sizes of Pd and Zn are similar; in the solids, Zn has filled metal−metal antibonding states from a filled 3d band, whereas the Pd 4d band is incompletely filled. Therefore, the lattice expansion from filling antibonding states and the size increase from going from the 4th to the 5th period are balanced between Zn and Pd.

Another viewpoint of the γ-brass structure is built of four condensed icosahedra;[44] the centers of these icosahedra are

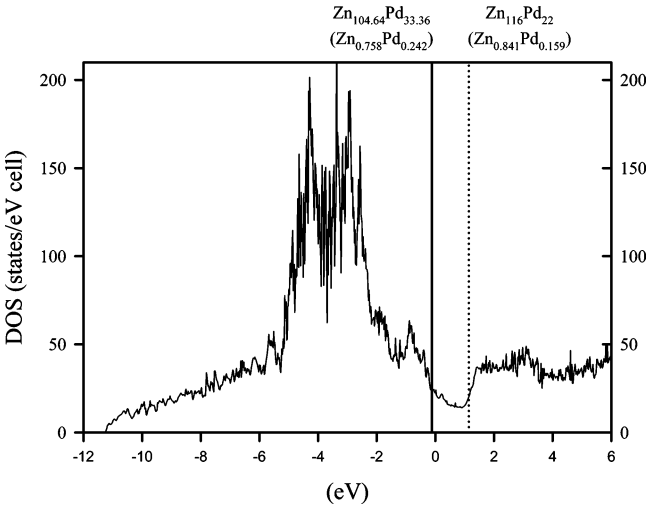

Figure 8. Total density of states for $Zn_{52.32}Pd_{16.68}$; Zn 3d orbitals are not included in this plot so that the behavior near the Fermi level, which is indicated by the solid line, can be highlighted. The dotted line is the Fermi level for $Zn_{58}Pd_{11}$ (15.9 at % Pd) and indicates the upper bound of the pseudogap using a rigid-band approximation.

the Pd sites. The calculated COHP curves[53] for Pd−Zn and Zn−Zn interactions in the γ-brass in Figure 7 show that Pd−Zn orbital interactions are optimized in this compound, whereas Zn−Zn are not, although the states near the Fermi level are weakly bonding. This provides an alternative interpretation to the pseudogap in γ-brasses, which we continue to study theoretically. In this Pd−Zn phase, the Pd−Zn bonding is optimized because the Zn 4s and 4p orbitals of the icosahedron overlap well with the valence 5s and 4d orbitals of Pd. The 4d orbitals are filled, and the 5s band shares electrons with the totally symmetric orbital of the icosahedron. The Pd−Zn bonding orbitals in these clusters are filled, whereas the Pd−Zn antibonding orbitals are empty. Optimal Pd−Zn bonding, according to the maximum ICOHP value, occurs very close to the observed composition of $Zn_{0.82}Pd_{0.18}$. Zn−Zn orbital interactions, on the other hand, would achieve an optimal bonding at 2.22 electrons per atom according to the COHP curve. It is interesting to notice that this value is the magic electron count for icosahedral quasicrystals and the Bergman phases.[2,7]

The density of states for the $Zn_{52.32}Pd_{16.68}$ phase is shown in Figure 8 and also shows a deep pseudogap for electron counts 1.516−1.682 valence s and p electrons per atom. This allows for a range of composition that is in excellent agreement with our observed phases. What this picture does not yet address is the complicated trend in lattice constants. Nevertheless, an earlier work by one of us shows that we can treat the Fibonacci system as a grouping together of two distinct structural and electronic building blocks.[24] The electronic specifications of the building blocks will lead to gaps (pseudogaps) in the theoretical electronic structure. Thus, there can be an electronic driving force for the observed lattice dimensions.

We can now use these two structures for the limiting compositions in this Zn−Pd system to identify these structural and electronic building blocks, which will allow us to interpret the intermediate compositions as possible

(52) Mann, J. B.; Meek, T. L.; Knight, E. T.; Capitani, J. F.; Allen, L. C. *J. Am. Chem. Soc.* **2000**, *122*, 5132.

(53) Dronskowski, R.; Blöchl, P. E. *J. Phys. Chem.* **1993**, *97*, 8617.

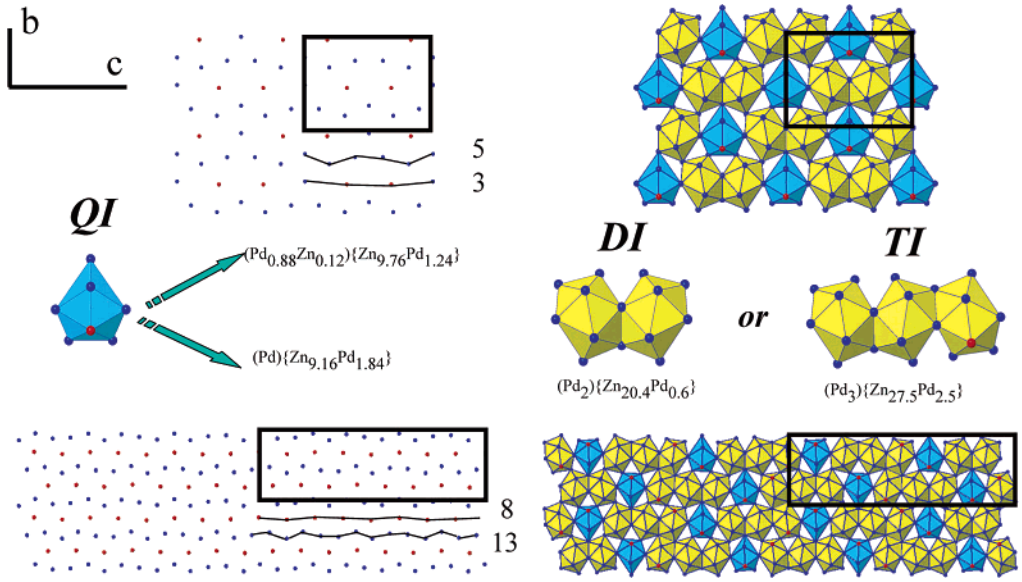

Figure 9. Illustration of the clusters DI ($Pd_2\{Zn_{20.4}Pd_{0.6}\}$) or TI ($Pd_3\{Zn_{7.5}Pd_{2.5}\}$) and QI that build the $Zn_{10.65}Pd_{2.35}$ structure (top) and the $Zn_{52.32}Pd_{16.68}$ structure (bottom part). The views of the pseudoperiodicities of the two different subnetworks are also illustrated.

intergrowth compounds and potential approximants to 1D quasicrystals. Figure 9 illustrates (010) projections in the $y = 1/4$ planes of the structures of $Zn_{10.65}Pd_{2.35}$ (γ-brass; orthorhombic setting) and $Zn_{52.32}Pd_{16.68}$. This figure highlights the important structure-building fragments: (i) two face-sharing icosahedra, $[Pd_2Zn_{21-n}M_n]$ (DI), from $Zn_{10.65}Pd_{2.35}$; (ii) three face-sharing icosahedra, $[Pd_3Zn_{30-n}M_n]$ (TI), from $Zn_{52.32}Pd_{16.68}$; and (iii) a spacer, $[MZn_{11-n}M_n]$ (QI), found in both structures (to represent these fragments, we have selected a distance cutoff of 2.90 Å. If we select a distance cutoff of 3.00 Å, then these chains consist of quasi-infinite, face-sharing (distorted) icosahedra). The DI unit has a mirror plane, so the fundamental length scale in the orthorhombic cell of the γ-brass structure is ···QI−DI···. On the other hand, the TI unit has an inversion center, which reverses the orientation of the QI units on each end, so the fundamental length scale in $Zn_{52.32}Pd_{16.68}$ is ···QI−TI−QI−TI···. In both structures, these clusters condense to form chains along the crystallographic c directions, and the corresponding layers are further condensed in an ···AB··· sequence to create full 3D structures.

As the left part of Figure 9 shows, these length scales can also be represented by the number of steps between cluster centers, n (3 and 8, respectively, in $Zn_{10.65}Pd_{2.35}$ and $Zn_{52.32}Pd_{16.68}$). Another step count occurs at the surfaces of the clusters, m (5 and 13, respectively, in $Zn_{10.65}Pd_{2.35}$ and $Zn_{52.32}Pd_{16.68}$). These two different step counts are evident in the diffraction studies during refinements of the lattice parameters: using the orthorhombic cells, the c^* component shows observed reflections for $l = pm + qn$ (p, q = integers; m, n = fundamental length scales). For example, observable reflections in $Zn_{52.32}Pd_{16.68}$ ($m = 13$, $n = 8$) will have $l = 13p + 8n$. It has already been pointed out that these step counts involve integers from the Fibonacci series.[22]

Analogies with the Fibonacci sequence are possible if we define the dimer unit DI as the short segment (S) and the trimer unit TI as the long segment (L), as in Table 1, but because of the inversion center in TI, we require two L segments. QI, which is a common unit in both compounds, corresponds to a spacer between segments. By defining these S and L segments, $Zn_{10.65}Pd_{2.35}$ and $Zn_{52.32}Pd_{16.68}$ correspond to the two first simplest approximants of a hypothetical 1D quasicrystal. This binary code of S and L segments may also be presented by a Farey tree,[54] which represents the rational number relationships within a certain defined interval. From one level (generation) to the next, the numerators and denominators, respectively, of the periodicities for two examples are added together to obtain the rational fraction for the subsequent generation. In Figure 10, the Farey tree begins with $Zn_{10.65}Pd_{2.35}$ (all S segments) and $Zn_{52.32}Pd_{16.68}$ (all L segments) as the extreme cases. The rational fraction (m/n) designates the periodicities of the two different chains described above. Intergrowth of these two structures can then be deduced using the tree. For example, first generation 5/3 (···S···) and 13/8 (···$L-L$···) go into the second generation 18/11 (···$S-L-L$···). Subsequently, a combination of a first generation 13/8 (···$L-L$···) and the second generation 18/11 (···$S-L-L$···) gives a third generation 31/19 (···$L-L-S-L-L$···) structure.

The unit cell length along these chains can then be approximated in two complementary ways: (1) $c = 4.3n$ Å, because the separation between metal atoms in the centers of DI, TI, and QI is nearly invariant (ca. 4.3 Å); or (2) c is the linear combination of the corresponding contributions of the S and L length scales according to the Farey tree: $D_S = d_{DI} + d_{QI}$ and $D_L = d_{TI} + d_{QI}$, so $c = n_S D_S + 2n_L D_L$ (n_S, n_L = integers). As a first approximation, we use $D_S = c(Zn_{10.65}Pd_{2.35}) = 12.912$ Å and $D_L = c(Zn_{52.32}Pd_{16.68}) = 33.32$ Å. There will be deviations due to the changes in composition, but as Table 2 shows, the agreement with our experimental determinations is quite good. We have observed from the refined unit cell parameters that the average volume per atom drops as the Pd content increases. In a fashion similar to that for the length of unit cell c parameter, we can approximate the optimal valence s and p electron

(54) *The Farey Series of Order 1025*; Royal Society Mathematical Tables, Vol. I; University Press: Cambridge, U.K., 1950.

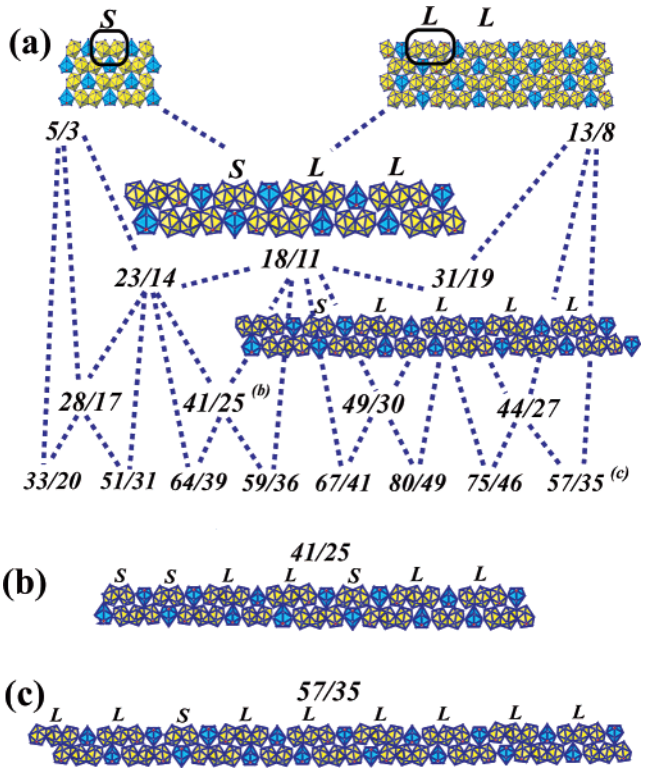

Figure 10. (a) Farey tree representation of the different hypothetical structures that may be obtained on the basis of parent compounds $Zn_{10.65}Pd_{2.35}$ and $Zn_{52.32}Pd_{16.68}$. The parent compounds define the short (*S*) and long (*L*) segment in the description of these as 1D approximant quasicrystalline phases. (b, c) Hypothetical atomic arrangements created on the basis of our sequence for the combinations 41/25 and 57/35, respectively.

concentration per atom (and, thus, the Zn/Pd composition) using the concept that we can use the weighted average of the valence electron concentrations for the two first generation structures. Therefore, $N_x = n_S N_{0.181} + n_L N_{0.242} = (1.642)n_S + (1.508)n_L$. These conclusions are also summarized in Table 2.

One essential characteristic of this Farey tree is the route converging toward the golden mean ratios of either *S*:*L* or *L*:*S*, which contain the fractions whose numerators and denominators are given by the Fibonacci numbers ($5/3 = F_5/F_4$ and $13/8 = F_7/F_6$ are two points along this route). With respect to the structural chemistry of this series, all crystalline examples constitute approximants to the fully quasiperiodic chains at the end of this tree. (There are so-called Fibonacci phases, which are periodic in two-dimensions and quasiperiodic in the third one, many of which are metastable or occur during the transition between icosahedral and crystalline or decagonal and crystalline phases;[55,56] however, to the best of our knowledge, none of the reported examples shows a series of approximants tending toward the Fibonacci phase.) As we have seen that the length scale and the valence electron concentration can be approximated using the algorithm set up by the Farey tree, can we predict the atomic structure of the more-complicated examples along this tree. Models of these structures are also illustrated in Figure 10. However, there remains sufficient structural flexibility to warrant a complete determination of these crystal structures, which will best be handled using superspace methods by generalizing the structure refinement using a simple modification of the modulated vector from phase to phase.[57] Such an analysis has been done recently on $CoZn_{7.8}$ by Lind et al. that partially confirms our thoughts.[58] An example of the possible structural possibilities is the case $Zn_{79}Pd_{21}$ (estimated as 41/25 on the Farey tree), which can show any of the following unit cell arrangements along the *c* direction: (1) ···*S*−*S*−*S*−*L*−*L*−*L*−*L*···; (2) ···*S*−*L*−*L*−*S*−*S*−*L*−*L*···; (3) ···*L*−*S*−*L*−*S*−*L*−*S*−*L*···; and (4) ···*S*−*L*−*S*−*S*−*L*−*L*−*L*···. Nevertheless, as the length scale increases, the new approximant becomes closer to a 1D quasicrystal. Therefore, the Farey tree allows us to target and synthesize as many new $Zn_{1-x}Pd_x$ phases as desired, if we are able to control the composition precisely. At present, we have identified six phases. In principle, we could synthesize 1D quasicrystal approximants as close as desired to the perfect Fibonacci sequence.

The study of Zn−Pd γ-brass phases is extremely promising as a way to further understanding of the relationships between intergrowth compounds, quasicrystals, and the possible electronic driving forces for their existence. The Farey tree representation implies the existence of numerous γ-brass phases in the Zn−Pd system, but keep in mind that the Farey tree representation is based on commensurate approximations, even if we suspect that incommensurate phases could exist. Nevertheless, such a representation, even if it may be restrictive to the commensurate cases, may be helpful for understanding the evolution new quasiperiodic or quasicrystalline structures.

Acknowledgment. The Ames Laboratory is operated for the U.S. Department of Energy by Iowa State University under Contract W-7405-ENG-82. This work was supported by the Office of Basic Energy Sciences, Materials Sciences Division of the U.S. Department of Energy. Also, a part of this work was supported by NSF Grants DMR-99-81766 and DMR-02-41092.

Supporting Information Available: Crystallographic information files and tables of anisotropic displacement parameters. This material is available free of charge via the Internet at http://pubs.acs.org.

CM0526415

(55) Steurer, W. In *Physical Metallurgy*, 4th ed.; Cahn, R. W.; Haasen, P., Eds.; North Holland Publishing: Amsterdam, 1996; p 372.
(56) Tsai, A. P.; Inoue, A.; Masumoto, T.; Sato, A.; Yamamoto, A. *Jpn. J. Appl. Phys.* **1992**, *31*, 970.
(57) Gourdon, O.; Petricek, V.; Evain, M. *Acta Crystallogr. Sect. B* **2000**, *56*, 409.
(58) Lind, H.; Boström, M.; Petricek, V.; Lidin, S. *Acta Crystallogr., Sect. B* **2003**, *59*, 720.